Distinct Genomic Aberrations Associated with *ERG* Rearranged Prostate Cancer

Francesca Demichelis,[1,2][†] Sunita R. Setlur,[3][†] Rameen Beroukhim,[4,5] Sven Perner,[1] Jan O. Korbel,[6]
Christopher J. LaFargue,[1] Dorothee Pflueger,[1,7] Cara Pina,[3] Matthias D. Hofer,[3] Andrea Sboner,[6]
Maria A. Svensson,[1] David S. Rickman,[1] Alex Urban,[8] Michael Snyder,[8] Matthew Meyerson,[4,5] Charles Lee,[3]
Mark B. Gerstein,[6,9,10] Rainer Kuefer,[7] and Mark A. Rubin[1]*

[1]Department of Pathology and Laboratory Medicine, Weill Cornell Medical Center, New York, NY 10065
[2]Institute for Computational Biomedicine, Weill Cornell Medical Center, New York, NY 10065
[3]Department of Pathology, Brigham and Women's Hospital, Harvard Medical School, Boston, MA 02115
[4]The Broad Institute of M.I.T. and Harvard, Cambridge, MA 02142
[5]Departments of Medical and Pediatric Oncology and Center for Cancer Genome Discovery,
Dana-Farber Cancer Institute, MA 02115
[6]Department of Molecular Biophysics and Biochemistry, Yale University, New Haven, CT 06520
[7]Department of Urology, University Hospital Ulm, Ulm D-89075, Germany
[8]Department of Molecular, Cellular, and Developmental Biology, Yale University, New Haven, CT 06520
[9]Interdepartmental Program in Computational Biology and Bioinformatics, Yale University, New Haven, CT 06520
[10]Department of Computer Science, Yale University, New Haven, CT 06520

Emerging molecular and clinical data suggest that ETS fusion prostate cancer represents a distinct molecular subclass, driven most commonly by a hormonally regulated promoter and characterized by an aggressive natural history. The study of the genomic landscape of prostate cancer in the light of ETS fusion events is required to understand the foundation of this molecularly and clinically distinct subtype. We performed genome-wide profiling of 49 primary prostate cancers and identified 20 recurrent chromosomal copy number aberrations, mainly occurring as genomic losses. Co-occurring events included losses at 19q13.32 and 1p22.1. We discovered three genomic events associated with *ERG* rearranged prostate cancer, affecting 6q, 7q, and 16q. 6q loss in nonrearranged prostate cancer is accompanied by gene expression deregulation in an independent dataset and by protein deregulation of MYO6. To analyze copy number alterations within the ETS genes, we performed a comprehensive analysis of all 27 ETS genes and of the 3 Mbp genomic area between *ERG* and *TMPRSS2* (21q) with an unprecedented resolution (30 bp). We demonstrate that high-resolution tiling arrays can be used to pin-point breakpoints leading to fusion events. This study provides further support to define a distinct molecular subtype of prostate cancer based on the presence of ETS gene rearrangements.   © 2009 Wiley-Liss, Inc.

INTRODUCTION

Recent discoveries in the field of prostate cancer have dramatically altered the understanding of the basic molecular mechanisms that underlie the progression of this heterogeneous disease. It is now well-established that the majority of prostate cancers harbor gene fusions involving the ETS family of transcription factors. The ETS gene family represents a highly conserved group of genes that were originally identified with the discovery of the v-ETS oncogene from the avian leukemia virus, E26, ERG (Leprince et al., 1983). The ETS family of transcription factors consists of 27 genes that share a highly conserved winged helix-turn-helix DNA binding domain (ETS domain). The biological function of ETS transcription factors is only incompletely understood, however, several of the ETS genes have been implicated in oncogenesis. The ETS transcription factors *FLI1* (Friend leukemia virus integration 1), *ETV1* (Ets variant gene 1), and *ERG* have been observed in gene rearrangements in leukemia, sarcoma, and prostate cancer. Following the discovery by Tomlins et al., reporting

recurrent fusions of the androgen-regulated gene *TMPRSS2* (Transmembrane protease, serine 2) and the transcription factors *ERG* and *ETV1* (Tomlins et al., 2005), subsequent studies showed additional fusions involving the ETS genes and various 5′ partners (Tomlins et al., 2006, 2007; Helgeson et al., 2008). In most cases, the ETS gene fusion partners act as upstream promoters driving the ETS gene expression.

Several pieces of evidence suggest that ETS fusion prostate cancers are a subclass of prostate cancer. First, *ERG* rearranged prostate cancers have a distinct expression signature (Setlur et al., 2008). Second, they have a more aggressive natural history as demonstrated by two independent Watchful Waiting cohorts (Demichelis et al., 2007; Attard et al., 2008), and third they are characterized by a distinct histological phenotype (Mosquera et al., 2007). However, the alterations at the genomic level (with the exception of deletion of the genomic segment between *TMPRSS2* and *ERG*) that might further characterize this subclass remain largely unexplored. To this end, we performed a genome-wide DNA analysis using Affymetrix 250 K SNP arrays to explore the somatic genomic alterations that might further serve to characterize this subclass and provide biological insights. We designed a high resolution NimbleGen tiling array to look for changes in the 27 ETS genes and to map genomic breakpoints. Collectively, we show strong evidence for specific genomic alterations associated with the *ERG* rearranged prostate cancer subclass.

MATERIALS AND METHODS

Patient Population

Prostate cancer samples and matched benign prostate tissue were taken from 51 men diagnosed with clinically localized prostate cancer between 2003 and 2004 at the Department of Urology, University of Ulm, (Ulm, Germany), where they underwent radical prostatectomy and pelvic lymph node dissection with curative intent. The samples were selected from a consecutive series based on adequacy of tumor density available material for SNP analysis. The patient population is comparable to the one above described (Hofer et al., 2006). All tumors were staged using the 2002 TNM system (Greenlee et al., 2001) and graded according to the revised Gleason Grading System (Amin et al., 2003). The distribution of the Gleason Grade in this population was

the following: 2% had Gleason Grade 5, 25% had Gleason Grade 6, 57% had Gleason Grade 7, 8% had Gleason Grade 8, and 8% had Gleason Grade 9. *ERG* rearrangement status was successfully evaluated for 50 samples by break-apart FISH test as in (Perner et al., 2006); 38% ($n = 19$) were negative and 62% ($n = 31$) were positive. Of the 31 *ERG* rearranged samples, 55% ($n = 17$) demonstrated deletion of *ERG* telomeric probe.

Cell line and Xenografts

The NCI-H660 cell line was obtained from the American tissue culture collection (ATCC, Manassas, Virginia) and was maintained according to the supplier's instructions. The Xenograft DNA was a kind gift from Dr. Robert Vassella, University of Washington, Seattle, Washington.

Dual-Color Interphase FISH Assays

To assess for *ERG* rearrangement, we performed a break-apart assay. For frozen material, a 5 μm section was cut and allowed to thaw at room temperature ($\sim$ 3–5 min). Slides were then fixed in 4% buffered formalin for 2 min and rinsed in 1× PBS. After fixation, slides were pretreated at 94°C in Tris/EDTA, pH 7.0, buffer for 0.5 hr before protein digestion with Zymed Digest-All (Invitrogen, Carlsbad, California) and ethanol dehydration. Following co-denaturation of the probes and samples (5 min at 75°C), slides were immediately placed in a dark moist chamber to hybridize for at least 16 hr at 37°C. After overnight hybridization, washing and color detection was performed as described earlier (Perner et al., 2006). Out of 51 frozen tissues, 50 were successfully evaluated.

To confirm the alterations of interest as identified through genome-wide profiling, two color interphase FISH assays were designed for specific loci on 16q, 7q, and 6q and performed on a set of 11 frozen samples (eight positive for *ERG* rearrangement and three negative). For 16q, BAC clones RP11-206B18 and RP11-662L15 were applied, targeting an area located at 16q23.1-23.2 containing the *MAF* gene. For 7q, BAC clone RP11-204M9 was applied, targeting an area located at 7q22.1 containing the *MCM7* gene. For 6q, BAC clone RP11-944L22 was applied, targeting an area located at 6q14.3 containing the *SNX14* gene. Reference probes were also used for each chromosome within a stable region identified by SNP array data (see above). For chromosomes 16, 7, and 6, the BAC clones used were RP11-309I14,

RP11-91E16, and RP11-943N14, respectively. All target probes were Biotin-14-dCTP labeled (eventually conjugated to produce a red signal), and all reference probes were Digoxigenin-11-dUTP labeled (eventually conjugated to produce a green signal). Correct chromosomal probe localization was confirmed on normal lymphocyte metaphase preparations. All BAC clones were obtained from the BACPAC Resource Center, Children's Hospital Oakland Research Institute (CHORI) (Oakland, California).

The samples were analyzed under a 60× oil immersion objective using an Olympus BX-511 fluorescence microscope, a CCD (charge-coupled device) camera, and the CytoVision FISH imaging and capturing software (Applied Imaging, San Jose, California). Semi-quantitative evaluation of the tests was independently performed by two evaluators (S.P., C.J.L.). For each case, we attempted to analyze at least 100 nuclei.

DNA Isolation

Areas enriched for tumor and benign tissue were identified and circled by the study pathologists (SP, MAR). Two biopsy cores, each 1.5 mm in diameter, were manually punched and placed in individual wells of a 96-well plate on dry ice. The tissue was lysed by incubating for 24–48 hr with lysis buffer (NaCl 100 mM, EDTA pH 8.5 25 mM, Tris pH 8.0 10 mM, SDS 0.5%) containing 1 mg/ml proteinase K (Ambion, Austin, Texas). Following this, automated DNA extraction was carried out using the CyBio liquid handling system. The DNA was extracted using equal volume of 25/24/1 phenol/chloroform/isoamyl alcohol. Isopropanol containing 0.7 M sodium perchlorate and 20 μg glycogen (Invitrogen, Carlsbad, California) was used for precipitation. Following a wash with 70% ethanol, the DNA pellet was resuspended and quantitated using Picogreen assay (Invitrogen, Carlsbad, California). 500 ng of DNA was used for the 250 K SNP array platform (Affymetrix, Santa Clara, California). DNA from the cell line was extracted using 10^6–10^7 cells using the phenol chloroform extraction procedure described above. The xenograft DNA was isolated using DNAzol (Molecular Research Center, Cincinnati, Ohio).

SNP Array Experiments and Data Analysis

Genomic DNA from paired cancer and benign prostate tissue from 51 individuals ($N = 102$) as well as from the NCI-H660 cell line and from the corresponding index case was hybridized to the 250 K Sty I chip of the 500 K Human Mapping Array set, Affymetrix Inc, which interrogates ∼ 238,000 SNP loci. Arrays were hybridized and scanned using the GeneChip Scanner 3000 at the core facility of the Broad Institute of MIT, Cambridge, Massachusetts. Probe level signal intensities were normalized using an invariant set of probes identified for each array against a baseline array (benign tissue sample). Normalized probe level intensities were then modeled using PM-MM difference modeling method (background removal) as in dChip (Li and Hung Wong, 2001) to obtain SNP level intensities. Three quality control steps were applied, based on genotype call rate (threshold was set at 85%), single sample intensity distribution, and assessment of genotype distances for all pair of samples within the dataset. The intensity distribution step evaluates if the tumor and normal samples exhibit the expected signal distribution, where genomic aberrations are expected to be present in tumors and not in normal samples. For a normal diploid sample, the excepted distribution for the log2 intensities is a one mode distribution centered in 1. In fact, when considering the entire genome signal distribution, germline copy number variations are expected to show minor signal variation (i.e., masked by the signal noise). The genotype distance evaluation implemented as in SPIA (Demichelis et al., 2008) ensures that there are no duplicates in the dataset and that the prostate cancer tissue and prostate normal tissue are correct matches. We then smoothed and segmented the log2 intensities using GLAD (Hupe et al., 2004) with d set equal to 10. A total of 49 primary tumor samples passed all quality control steps and were included in final analysis.

To detect potential recurrent changes concordant across the dataset and therefore less likely to be random passenger events, we applied GISTIC (Beroukhim et al., 2007) to our segmented dataset. Briefly, this approach considers frequency and dosage of variation across the genome and ultimately assigns a Q-value to each locus, reflecting the possibility that the event is due to fluctuations. The statistical evaluation for the significance is separately performed for amplifications and losses. The analysis generates a list of significant recurrent changes, each characterized by change peak boundaries and corresponding Q-value (threshold set to 0.25). To meaningfully apply this approach to our data and extract consistent information, we needed to define a threshold on the intensity signal to

distinguish between noise fluctuation and biological signal variation. We reasoned that the appropriate way was to use prior knowledge on the well characterized interstitial deletion in chromosome band 21q22 (Perner et al., 2006). We identified the samples annotated as *ERG* rearrangement positive with deletion of the *ERG* telomeric probe by FISH test and showing presence of deletion by SNP data. We then selected the one with the lowest absolute value of the log2 intensity ratio and set the threshold to that value. Association between lesions (presence or absence) and between single lesion and phenotype was evaluated by Fisher exact test. All *P* values are two-sided, unless otherwise specified.

Custom ETS Fusion Prostate Cancer Tiling Array Design and Experiments and Breakpoint Identification

Tiling arrays allow for high-resolution mapping of copy number genomic polymorphisms, including small to moderately sized (0.5–10 kb) deletions and insertions, across large regions of the human genome using total genomic DNA (Urban et al., 2006). Oligonucleotide arrays with 385,000 features can be synthesized by photolithography; by tiling large segments of genomic DNA, these arrays have the potential to map deletions at very high resolution. In addition, the sensitivity of suitably designed arrays is sufficiently high that total genomic DNA can be directly hybridized, thus avoiding bias that arises during selective PCR amplification of subsets of the DNA.

We designed a custom tiling path NimbleGen array for the study of ETS fusion prostate cancer. We prioritized high resolution coverage for the ETS gene regions (average intermarker distance $\sim$ 30 bp) and for the $\sim$ 3 Mbp area between *ERG* and *TMPRSS2* on chromosome arm 21q (average intermarker distance $\sim$ 20 bp). Regions previously reported to be associated with prostate cancer were also included on the chip at $\sim$ 2.6 Kbp resolution. Two control regions were also included in the design to be used as zero state reference (chr12: 99,000,001-102,000,000 and chr19:14,500,001-20,000,000 location), at a resolution of $\sim$ 2 Kbp. Four samples were hybridized on the ETS fusion prostate cancer tiling array: 1 blood sample (NA12156), 1 cell line (NCI-H660), 2 xenografts (LuCaP86.2 and LuCaP35), and one tissue sample (LN13, lymphonode). All prostate cancer samples were positive for *TMPRSS2-ERG* rearrangement (Perner et al., 2006). In addition, LuCap93 was hybridized on tiling array as in Urban et al., (2006). All of the experiments were carried out at Nimble-Gen Systems, Reykjavik, Iceland.

Data analysis

Fluorescence intensity raw data were obtained from scanned images of the oligonucleotide tiling arrays by using NIMBLESCAN 2.3 extraction software (NimbleGen Systems). For each spot on the array, log2-ratios of the Cy3-labeled test sample versus the Cy5-labeled reference sample were calculated. Because of the highly skewed design toward prostate cancer aberrations, the single sample data were not conventionally normalized, but subtracted by the median value of the log2 intensity ratios of the two control regions. For visualization purposes, tiling array data are smoothed using a pseudo-median approach (Royce et al., 2007). Here we used a sliding window of 100 markers.

Breakpoint Identification

The tiling array data were analyzed for breakpoints using BreakPtr algorithm (Korbel et al., 2007). This is described in the supplemental materials. Vectorette PCR amplification system (Sigma-Aldrich, St. Louis, Missouri) was used to identify the *TMPRSS2-ERG* fusion breakpoint. Briefly, 2 μg of DNA were digested using EcoRI/HindIII restriction enzymes and cloned into vectorette units which contain adapter sequences of the corresponding restriction enzymes. The coordinates from the analysis were used to design sequence specific primers for PCR. The ligated vecorette libraries were used as templates for PCR reactions with the sequence specific primer (ERGVEC_FWD_PRIMER8: 5'AGAAGCCTCC-CAAATCTGTATCTTATGG 3') and the reverse vectorette primer. The products were sequenced using the sequence specific primer at MWG biotech, Highpoint, North Carolina.

Genomic Location Enrichment Analysis for Transcript Data

To study the potential genome location enrichment for ETS fusion related genes, we analyzed two prostate cancer gene expression datasets, annotated for *ERG* rearrangement. We focused on fusion genes selected through consensus procedure for association with prostate cancer rearrangement status: genes selected more than 5% out of 100 iterations. We applied consensus gene
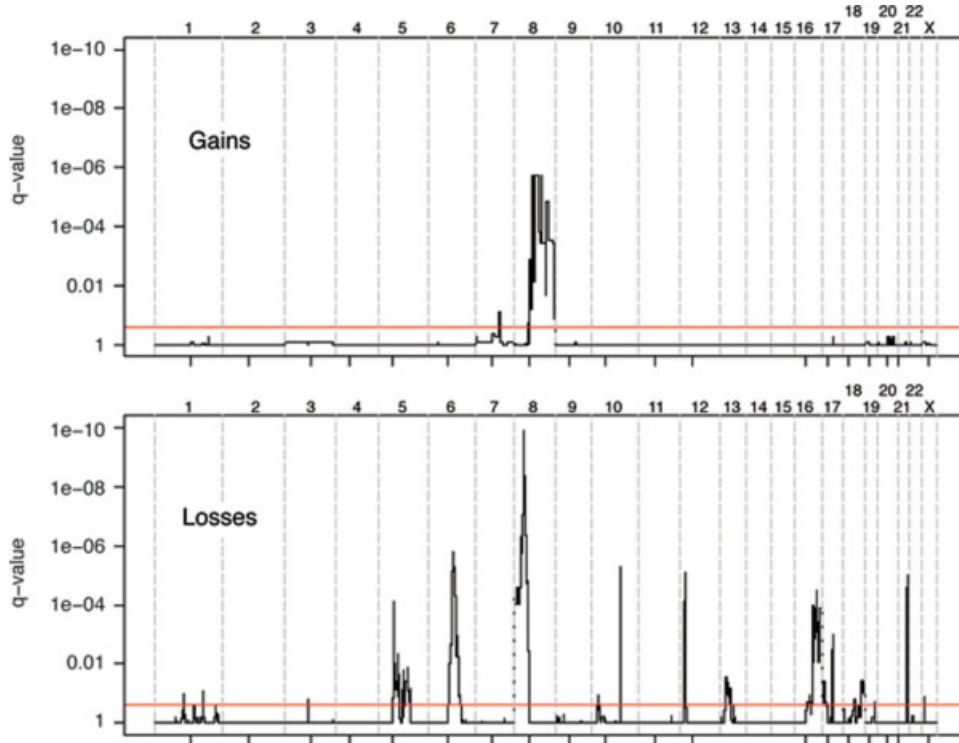
Figure 1. Genomic aberrations in primary prostate cancers as evaluated on a collection of 49 samples. The red lines identify *Q*-values of 0.25 as cutoff for significance. Q-values are plotted along the genomic location, with chromosomes delineated by vertical dotted lines and centromeres by small marks. The top frame refers to gains (amplification) and the lower frame to losses (deletions).

selection procedure as in JCNI (Setlur et al., 2008). Briefly, we repeated 10 splits of 10-fold cross validation of *t* test, with $P < 0.00005$ (SW) and $P < 0.001$ (PHS) as thresholds, respectively. The enrichment analysis (using 5% as fusion gene selection threshold) included 233 (SW) and 107 (PHS) genes associated with *ERG* rearrangement (162 and 71, and 48 and 59 down-regulated and up-regulated genes, respectively). We defined the enrichment score as: $\text{ES}_{region} = (\text{NfusionGenes}_{region} / \text{NfusionGenes}) / (\text{NGenes}_{region} / \text{NGenes})$. Region can be chromosome or chromosomal arm. ES_{region} greater than one indicates that the region is enriched for rearrangement associated genes. Maximum enrichment score occurs when all genes in the region of interest are all of the genes associated with the rearrangement (for SW would be 48). We applied *P* values by means of Hypergeometric distribution.

Immunohistochemistry for MYO6

Paraffin-embedded tissue microarray section, 4 μm thick, was deparaffinated and rehydrated using xylene and graded ethanol, respectively.

Pressure cooking with citrate buffer (pH 6.0) for 10 min was used as antigen retrieval method. Primary antibody Myosin VI, 1:50 dilution (mouse monoclonal, clone MUD-19, Sigma-Aldrich, Saint Louis, Missouri) was stained on the Leica Microsystems Bond-Max Autostainer using DakoCytomation Envision and System Labeled Polymer HRP anti-mouse (K4001). Evaluation of the protein expression was performed by visual inspection (MAR).

RESULTS

Recurrent Aberrations in Primary Prostate Cancer

To determine the genomic landscape of primary prostate cancer and identify recurrent copy number alterations, we successfully profiled 49 well-annotated tumors using the high-density genome-wide Affymetrix platform, querying $\sim 238{,}000$ loci. To distinguish somatic changes from germline structural variations, we normalized tumor DNA signal to normal prostate DNA signal generated from the same individual. Our analysis detected 20 recurrent events with frequencies ranging from
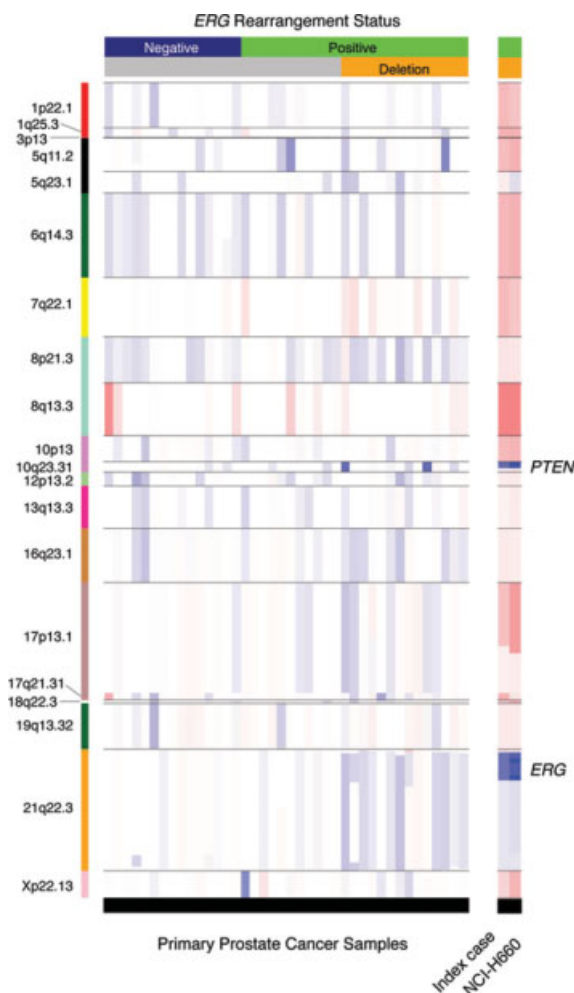
Figure 2. Smoothed segmented copy number data of recurrent lesions. The heatmap shows log2 intensity ratios within the detected recurrent lesions (annotated by chromosome band on the left side). The 40 prostate cancer samples harboring the recurrent lesions are presented, ordered based on *ERG* rearrangement status (upper horizontal bar) and by deletion status of *ERG* telomeric probe as assessed by dual-color FISH. The right hand profiles show the genomic status of the same regions in NCI-H660 cell line and in the corresponding index case (prostate cancer metastasis). Red and blue colors indicate gains and losses, respectively. Color intensity corresponds to copy number change amplitude. White indicates no change.

10 to 43%. Ninety percent of the events (18 out of 20) were losses, with loss at 8p21.3 and 6q14.3 being the most common alterations. A minority of recurrent events ($n = 2$) were gains, located at 8q13.3 and 7q22.1, with low to moderate copy number increases. Nine samples did not show any of these distinct recurrent lesions, and were characterized by only a weak aberrant signal. The genome-wide profile for gains and losses evaluated in our tumor cohort is shown in Figure 1, where the most significant genomic changes are represented by lower *Q*-value. Statistically significant recurrent events are listed in Supporting information Table 1. Interestingly, some events tend to co-occur (see Fig. 2). All 19q13.32 losses ($N = 5$) occur in the presence of 1p22.1 loss (Fisher exact test *P* value < 0.001). Similarly, losses on 17q21.31 and on 21q22.3 co-occur with losses on 18q22.3 and 16q23.1, respectively (Fisher exact test *P* values of 0.004 and 0.001). A comparison between these findings and genomic aberrations previously detected by our group on more advanced tumor samples profiled using 100 K Affymetrix Array (Perner et al., 2006) indicates overall agreement and suggests that prostate tumors accumulate gains over time (see Supp. Info. Fig. 1).

Genomic Aberrations Characteristic of *ERG* Rearranged Prostate Cancer

We recently demonstrated that *ERG* rearranged prostate cancers are characterized by an 87 gene signature (Setlur et al., 2008), supporting the view that these tumors belong to a distinct subclass. Other than the common interstitial deletion between *ERG* and *TMPRSS2* (21q22 deletion) (Perner et al., 2006), we observed that *ERG* rearranged and *ERG* nonrearranged prostate cancer do not differ in terms of overall frequency of copy number alterations, with an average number of lesions being 4.4 ± 2.7 and 3.5 ± 2.5, respectively. Of the 20 recurrent events, three showed significant association with *ERG* rearranged genotype: gain on 7q (*P* value = 0.04) and deletion on 16q (*P* value = 0.04), enriched in rearranged cases and deletion on 6q (*P* value = 0.02), enriched in nonrearranged cases. Figure 3a demonstrates the presence or absence of these three lesions for the 40 cases which showed recurrent aberrations, sorted with respect to *ERG* rearrangement status. The combination of losses on 16q and 6q accounts for 75% of *ERG* rearranged cases. In our series, we did not detect any association between *ERG* rearrangement and *PTEN* (*Phosphatase and tensin homologue (mutated in multiple advanced cancers 1)*) loss. Decreased copy number of *PTEN* was seen in 16% of the cases (with two cases showing loss of both copies), a much lower frequency than recently reported by Yoshimoto et al. (2007).

The genomic profile of the *TMPRSS2-ERG* fusion positive NCI-H660 cell line (Mertz et al., 2007), derived from a pulmonary metastasis of an aggressive small cell carcinoma of the prostate, shows characteristic deletions of 21q22 and *PTEN* locus (10q23) and abundant amplifications in the most commonly altered prostate cancer loci (see right hand side of Fig. 2). Multicolor
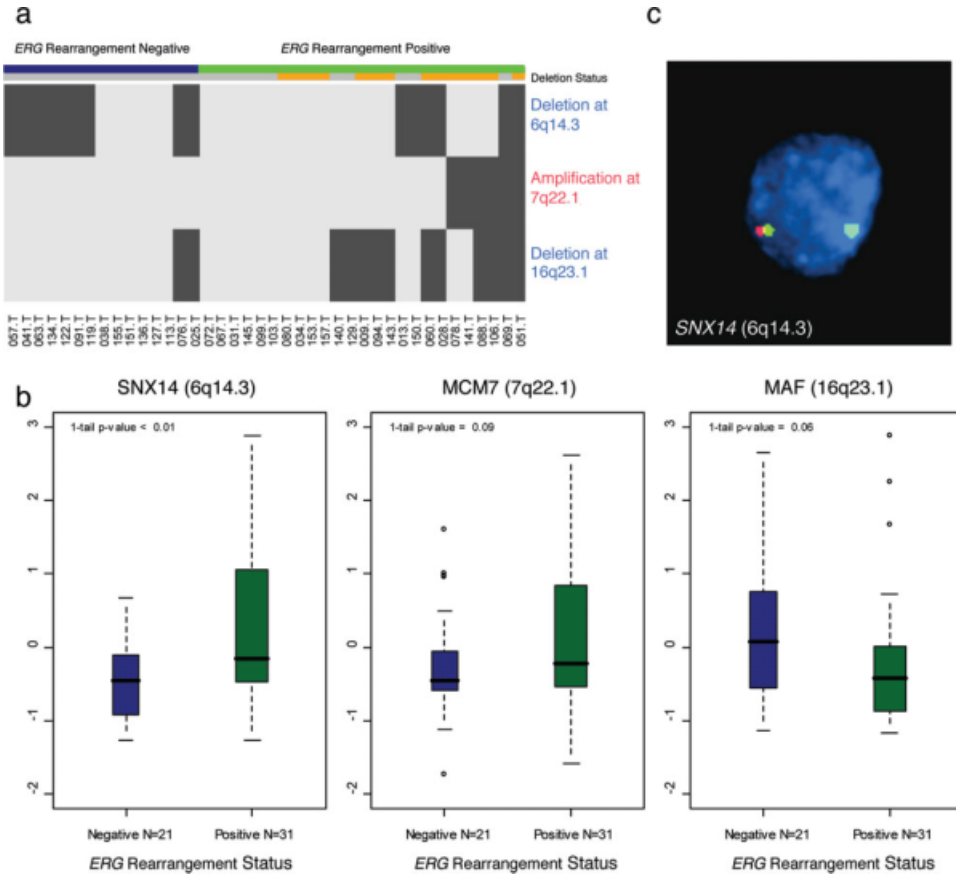
Figure 3. *ERG* rearranged prostate cancer lesions. (a) Binary representation of three genomic recurrent lesions associated with *ERG* rearranged prostate cancer (gray indicates absence, black indicates presence of lesion). The samples are sorted by *ERG* rearrangement status and annotated for deletion status of *ERG* telomeric probe as assessed by dual-color FISH. (b) Distributions of transcript expression of *SNX14*, *MCM7*, and *MAF* genes in two sets of *ERG* rearranged negative and *ERG* rearranged positive prostate cancers as determined by expression profiling. The genes were selected as centrally located in the three fusion associated lesions. (c) Monoallelic deletion for *SNX14* in primary prostate cancer cell as determined by FISH. A representative tumor nucleus demonstrates the loss of a red probe at 6q14.3.

FISH (M-FISH) was performed on the NCI-H660 cell line revealing a complex karyotype presumably due to a high degree of genomic instability. In addition, 50% of the cells analyzed were hyperdiploid and the rest were polyploid (consistent with whole chromosome gains observed in the SNP data), with the exception of chromosomes 21 and X. Chromosome Y was seen to be lost (Supp. Info. Fig. 2).

In Situ Validation

To validate the recurrent lesions associated with the rearranged cancer subclass, we chose genes within the area of maximum statistical confidence and prioritized genes that were demonstrated to be functionally important in cancer progression. For the in situ validation, we performed FISH test to assess for copy number alterations of *SNX14* (sorting nexin 14) (Fig. 3c),

MCM7 (Minichromosome maintenance complex component 7), and *MAF* (v-maf musculoaponeurotic fibrosarcoma oncogene homologue (avian)) located in the peak lesions of 6q, 7q, and 16q on a selection of samples ($N = 11$). We were able to confirm all three aberrations (the concordances between SNP data and FISH were 82%, 73%, and 73%) (data not shown). In few cases we observed mosaicism (presence of two populations of cells with different genotypes in one individual), where approximately 20% of the tumor cells showed aberration. This phenomenon may help to explain the low signal variations observed in the SNP data.

To assess whether these genomic aberrations affect the gene transcripts, we interrogated a set of 52 primary prostate cancers (Rickman and Rubin, unpublished data), focusing on *SNX14*, *MCM7*, and *MAF* mRNA levels and observed expected trends (Fig. 3b), where *SNX14* and *MCM7* tend to be

over-expressed (with *P* values < 0.01 and 0.09-1-tail) in *ERG* rearranged cases and *MAF* tends to be down-regulated (*P* value = 0.06, 1-tail).

Analysis of Rearrangement Related Gene Expression for Chromosome/Arm Enrichment

Cooperative changes in gene expression levels might be initiated by genomic alterations, as gains or losses, by other nongenomic mechanisms such as transcriptional regulation, or by their combination. Orthogonal datasets of well annotated tissue samples are needed to investigate potential mechanism on large scale. To investigate genomic areas enriched for *ERG* rearrangement associated transcripts, we analyzed two prostate cancer datasets annotated for *ERG* rearrangement by FISH analysis and then compared with the results with *ERG* rearrangement associated genomic aberrations. One cohort includes 354 individuals from Sweden (SW) and a second cohort includes 101 individuals from the US (Physician Health Study, PHS) (for details on the cohorts see Setlur et al., (Setlur et al., 2008)). The expression array data set is accessible through GEO—(http://www.ncbi.nlm.nih.gov/geo/).

When evaluating chromosomal and chromosomal arm enrichment, we detected significant enrichment values for chromosomes 6 (PHS, *P* < 0.007), 14 (SW, *P* < 0.01) and 21 (PHS, *P* < 0.05), and for 6p (PHS, *P* < 0.05), 6q (PHS, *P* < 0.04), 14q (SW, *P* < 0.01), and 21q (PHS, *P* < 0.05). When considering the deregulation direction (over- or under-expression with respect to *ERG* rearrangement genotype), we measured significant enrichment scores for over-expression on 2p (SW, *P* < 0.009), 6p (PHS, *P* < 0.009), 6q (SW, *P* < 0.009 and PHS, *P* < 0.01), and 14q (SW, *P* < 0.001). Significant enrichment scores for under-expression are detected on 18p (PHS, *P* < 0.03) and 21q (PHS, *Q* < 0.04).

Figure 4a shows the enrichment scores as evaluated for p- and q-arms of each chromosome (*x*-axis) for the two cohorts, distinguishing between up-regulated and down-regulated rearrangement genes. Only significant *P* values are reported. Of interest, chromosome arm 6q is consistently scored significant for enrichment of up-regulated rearrangement-related genes in the two cohorts. The detected genes located on 6q are *MYO6* (Myosin VI), *SNAP91* (Synaptosomal-associated protein, 91kDa homologue (mouse), *AMD1* (Adenosylmethionine decarboxylase 1), *HDAC2* (Histone deacetylase 2), *MAP3K5* (Mitogen-acti-vated protein kinase kinase kinase 5), *PREP* (Prolyl endopeptidase), *PTPRK* (Protein tyrosine phosphatase, receptor type, K), *SMPDL3A* (Sphingomyelin phosphodiesterase, acid-like 3A), *MAP7* (Microtubule-associated protein 7), *TBP* (TATA box binding protein).

MYO6 was one of the genes included in the 87 gene signature as being up-regulated in *ERG* rearranged prostate cancers (1-tail *P* value = 2.0e-7, see boxplot in Fig. 4b) and has been previously implicated as being over expressed in prostate cancer, particularly in higher grade disease (Wei et al., 2008). On an independent set of primary prostate cancers (*N* = 16), half showing *ERG* rearrangement and half without *ERG* rearrangement, we evaluated MYO6 protein expression (Fig. 4c, see Supp. Info. materials). We observed a direct association between over-expression of MYO6 protein and *ERG* rearrangement status (Fisher exact test, *P* value = 0.04).

Genomic Aberrations of ETS Genes: The Use of Tiling Arrays for Breakpoint Analysis

The 250 K Sty SNP Array offers coverage (more than 5 markers) for a subset of ETS genes, namely *ELF5 (*E74-like factor 5 ESE-2), *EHF* (Ets homologous factor), *ETS1* (V-Ets erythroblastosis virus E26 oncogene homologue 1 (avian)), *ETV6* (Ets variant gene 6 (*TEL* oncogene)), and *ERG* (Fig. 5a). Interestingly, *ETV6*, the largest among the ETS genes, undergoes hemizygous deletion in about 25% of prostate cancers. *ERG*, the most frequent ETS gene involved in fusion event with the androgen-regulated *TMPRSS2* gene, is represented by 31 SNP markers. As previously reported (Liu et al., 2006; Perner et al., 2006), the interstitial genomic lesion which accounts for about half of *TMPRSS2-ERG* fusion prostate cancers exhibits a heterogeneous starting location (Fig. 5a). To better investigate the extent of aberrations of the ETS genes and to pin-point *TMPRSS2-ERG* rearrangements, we designed a custom tiling array chip with one marker every 20–30 bp on areas of interest (see Supp. Info.Table 2) and profiled four prostate cancer samples.

Figures 5b and 5c show smoothed log2 ratio signals for four prostate cancer samples and one control (NA12156, top frames). The heterogeneity of the interstitial deletion between *ERG* and *TMPRSS2* is highlighted in these four samples. LuCap35 is characterized by homozygous deletion of *ERG* and of centromeric portion of *ETS2* (39150
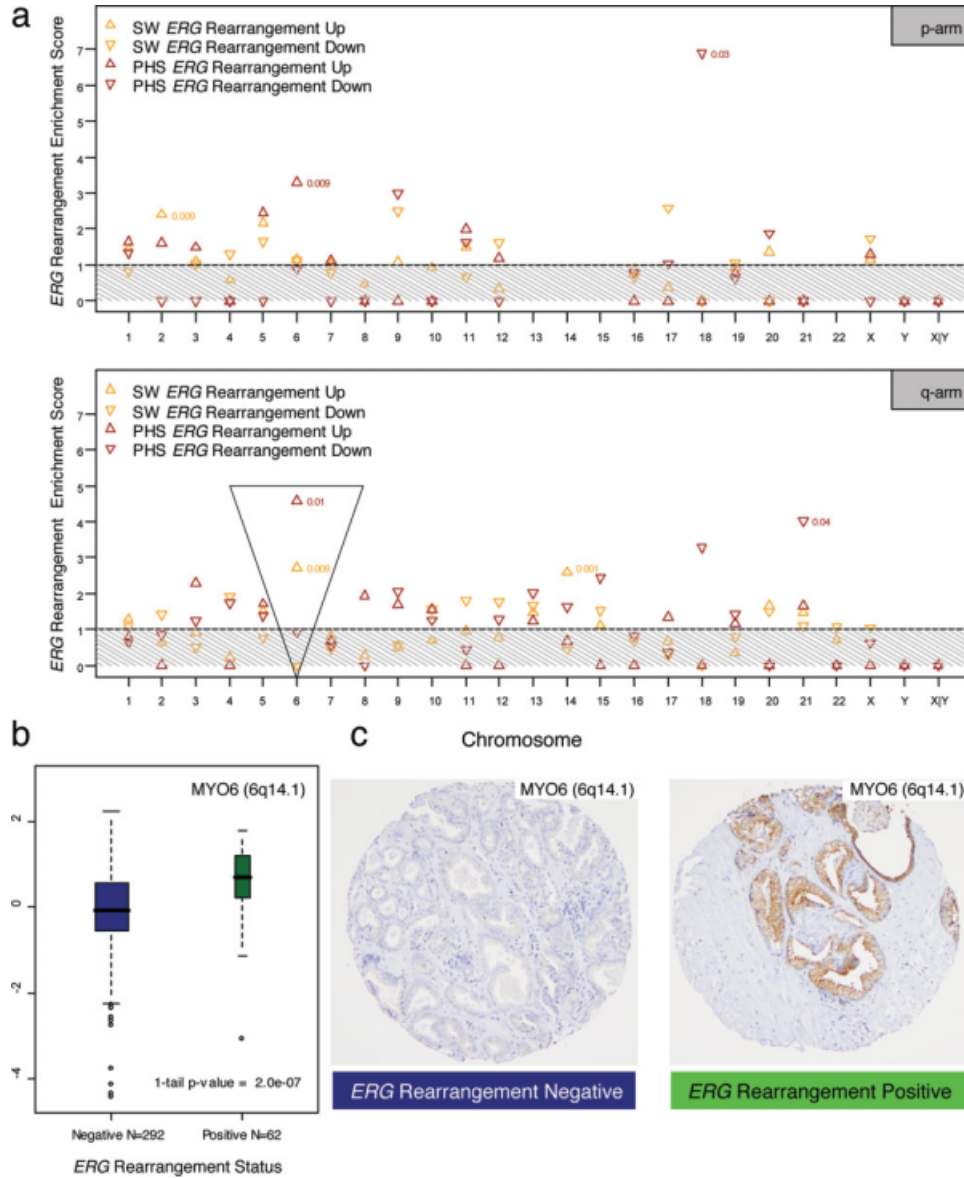
Figure 4. Chromosomal arm enrichment for *ERG* rearrangement related genes. Two prostate cancer gene expression datasets annotated for *ERG* rearrangement by FISH analysis were analyzed and compared with genomic aberrations. (a) *ERG* rearrangement enrichment scores derived by gene expression data are presented on *y*-axis for p and q arms for each chromosome (*x*-axis). Maximum enrichment score occurs when all genes on a specific arm are associated with rearrangement status. The two cohorts (see text for details) are color coded and directionality of deregulation versus rearrangement status is represented by up and down arrows. Significant *P* values, evaluated by the Hypergeometric distribution, are shown. Significant enrichment scores for over-expression were detected for 2p (SW, *P* < 0.009), 6p (PHS, *P* < 0.009), 6q (SW, *P* < 0.009 and PHS, *P* < 0.01), and 14q (SW, *P* < 0.001). Significant enrichment scores for under-expression are detected on 18p (PHS, *P* < 0.03), and 21q (PHS, *Q* <0.04). Interestingly, the 6q arm is consistently scored significant for enrichment of up-regulated rearrangement-related genes in the two cohorts and was shown to harbor a genomic deletion in fusion negative cancers. (b) *MYO6* (Myosin VI) located 6q14.1 and deregulated in rearrangement positive cancers (see boxplot, left). (c) We observed a direct association between over-expression of MYO6 protein (immunohistochemistry evaluation on a tissue microarray, right) and *ERG* rearrangement status (Fisher exact test *P* value = 0.04).

Kb) and by hemizygous deletion from *ETS2* to PCP4 (Purkinje cell protein 4) (from 39,150 Kb to 40,320 Kb). The NCI-H660 cell line shows homozygous deletion starting at exon 4 of *ERG* to *ETS2* (from 38,786 Kb to 39,440 Kb), followed by hemizygous deletion to *TMPRSS2*. The high signal variance shown by the cell line is likely explainable by a complex karyotype revealed by M-FISH analysis (See Supp. Info. Fig. 2). The homozygous deletion observed in NCI-H660 was previously confirmed by FISH (Fig. 5d; see also SNP data analysis in Fig. 2).
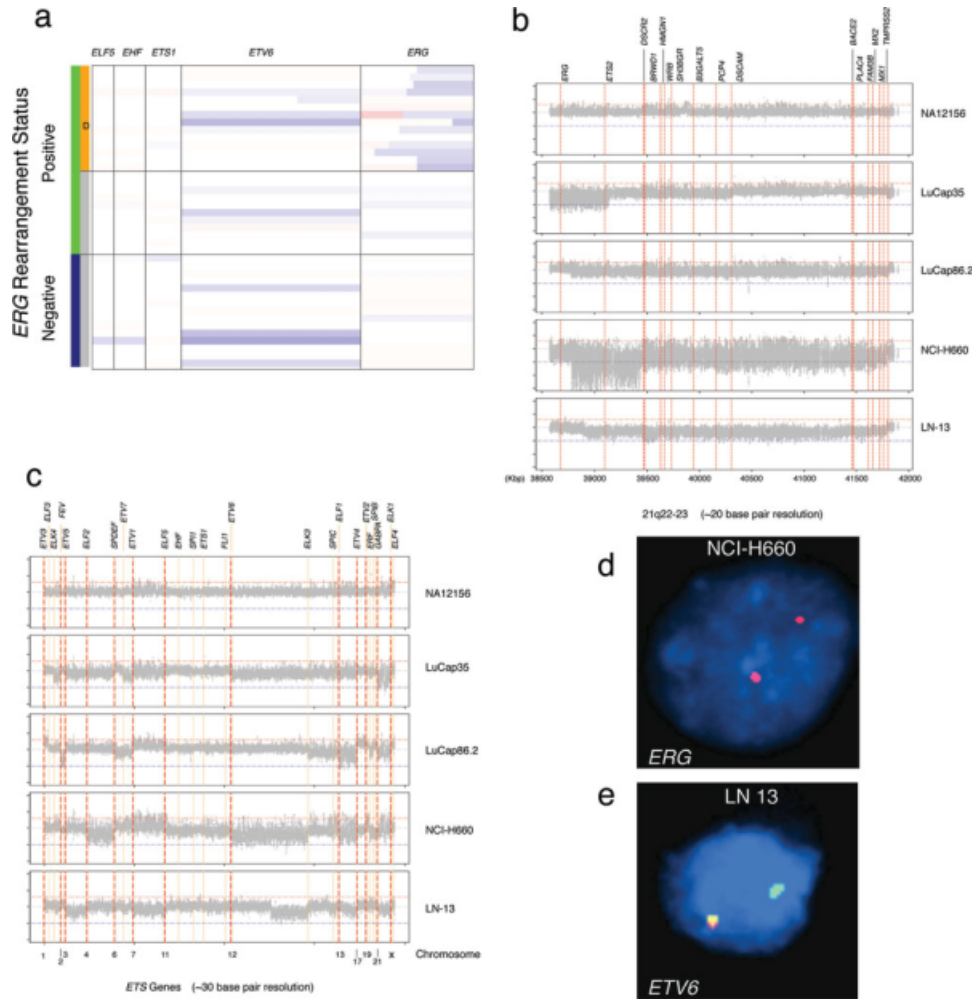
Figure 5. Genomic aberrations of ETS genes. (a) 250 K Sty SNP Array data for a subset of ETS genes, (i.e., *ELF5*, *EHF*, *ETS1*, *ETV6*, and *ERG*) are presented. *ETV6* undergoes hemizygous deletion in about 25% of prostate cancers. *ERG* is represented by 31 SNP markers and demonstrates an interstitial genomic lesion in approximately half of *ERG* rearranged prostate cancers. (b, c) Custom ETS gene tiling arrays with one marker every 20–30 bp were used on four prostate cancer samples. Smoothed log2 ratio signals for the four prostate cancer samples and one control (top frames) demonstrate the heterogeneity of the interstitial deletion between *ERG* and *TMPRSS2* as seen in panel b. LuCap35 is characterized by homozygous deletion of *ERG* and of centromeric portion of *ETS2* (39,150 Kb) and by hemizygous deletion from *ETS2* to *PCP4* (Purkinje cell protein 4) (from 39,150 Kb to 40,320 Kb). The NCI-H660 cell line shows homozygous deletion starting at exon 4 of *ERG* to *ETS2* (from 38,786 Kb to 39,440 Kb), followed by hemizygous deletion to *TMPRSS2*. The homozygous deletion observed in NCI-H660, was confirmed by FISH (d). In panel c, the remaining ETS genes were analyzed. We observed that the hormone naÿve metastatic lymph node sample (LN13) demonstrated a partial deletion of *ETV6*, the second most commonly altered ETS gene, starting at 11,813,084 bp (chromosome 12). FISH analysis validated the deletion of the telomeric end of *ETV6* (e). In addition to *ERG*, *ETS2*, and *ETV6*, we observed aberrations of other ETS genes (i.e., *FEV*, *ELF1*, and *ERF*).

When querying all the ETS genes, we observed that the hormone naÿve metastatic lymph node sample (LN13) shows a partial deletion of *ETV6*, the second most commonly altered ETS gene, starting at 11,813,084 bp (chromosome 12). FISH analysis validated the deletion of the telomeric end of *ETV6* (Fig. 5e). In addition to *ERG*, *ETS2*, and *ETV6*, we observed aberrations of other ETS genes (see Supp. Info. Table 2), such as *FEV* (ETS oncogene family), *ELF1* (E74-like factor 1 (ets domain transcription factor)), and *ERF* (Ets2 repressor factor).

One major advantage of using a high resolution tiling array is that by narrowing down the breakpoint area, we would be able to identify precise fusion location, as suggested by Korbel et al. (2007). This approach would allow for efficient identification and characterization of various breakpoints observed in the *TMPRSS2-ERG* fusion. Here we present one example as proof of principle, where we were able to demonstrate the fusion breakpoint for LuCap93 xenograft. By applying BreakPtr to the tiling array data we identified the two putative breakpoint areas at

38,804,000 ± 1,000 bp and 41,792,500 ± 2,500 bp. This information was used to design a series of primers to identify the exact breakpoint using the vectorette PCR approach and sequencing (Korbel et al., 2007). Supporting Information Figure 3 shows the log2 intensity ratio of the area of interest between *TMPRSS2* and *ERG* in the fusion positive xenograft (Panel A), LuCaP 93 and the breakpoint sequencing data (Panel B). The breakpoints were found to be located in introns 3 (Genomic position 38,802,313 bp) and 1 (Genomic position 41,794,772 bp) of *ERG* and *TMPRSS2*, respectively. The detection of fusion isoform expression as evaluated by RT-PCR showed presence of isoform 3, consistent with the DNA breakpoint (Panel C).

DISCUSSION

Somatic copy number alterations have been shown to be associated with prostate cancer (Saramaki and Visakorpi, 2007). Reported alterations include amplifications of 7q and 8q and deletions of 5q, 6q, 8p, 13q, 16q, 17p, and 18q. These cancer associated chromosomal alterations have been recapitulated in our dataset where we see an accumulation of aberrations with cancer progression. Our observations are in agreement with a recent study from Lapointe et al. (2007), which showed higher number of losses versus gains and accumulation of genomic aberrations in lymph node metastases. A few samples did not show any of the recurrent changes suggesting that nongenomic alterations (epigenetic, transcriptional, and translational) might be responsible for tumorigenesis in these samples. The confounding limitation of stromal contamination has been addressed by exclusion of cases from which infiltrating tumor cells could not be reliably dissected from the surrounding nontumor tissue. Importantly, this study elucidates the landscape of chromosomal aberrations in the context of fusion prostate cancer, a distinct subclass defined most commonly by fusion of the androgen *TMPRSS2* gene and the ETS transcription factor *ERG*.

High resolution SNP arrays were used to identify common molecular alterations to help distinguish *ERG* rearranged prostate cancers from nonrearranged prostate cancer. Comparison of the absolute number of lesions detected in nonrearranged cancer versus rearranged cancer did not show a statistically significant difference. This may indicate either that the sample number is limiting or that, number of lesions being equal,

separate genomic alterations may be responsible for tumor onset and progression in each of the subclasses. Further, the subclass specific lesions might define the clinical outcome. Although a few of the identified alterations have been shown earlier to be associated with prostate cancer, our study demonstrates that these changes occur specifically in the rearranged or nonrearranged subclasses of prostate cancer.

The loss of 16q has been previously reported to be associated with prostate cancer (Saramaki and Visakorpi, 2007). This loss was seen to occur at a frequency as high as 50% which is similar to the frequency of reported *TMPRSS2-ERG* fusions in prostate cancer (Matsuyama et al., 2003; Saramaki et al., 2006). The frequency of deletions at 16q24 has also been reported to increase with cancer progression and with metastasis incidence (Matsuyama et al., 2003). Our study demonstrates the specific association of this alteration with the *ERG* rearranged cancer subclass. Several genes in this area have been implicated to have a tumor suppressor role, with loss leading to cancer progression. The candidate genes that have been reported include *MAF* (v-maf musculoaponeurotic fibrosarcoma oncogene), *ATBF1* (AT-binding transcription factor 1), *FOXF1* (forkhead box F1), *MVD* (mevalonate (diphospho) decarboxylase), *WFDC1* (WAP four-disulfide core domain 1), *WWOX* (WW domain containing oxidoreductase), *CDH13* (Cadherin 13), and *CRISPLD2*, (cysteine-rich secretory protein LCCL domain containing 2) (Watson et al., 2004; Saramaki and Visakorpi, 2007). We validated the expression of *MAF* in our cohort and found its expression to be concomitantly down-regulated in the rearranged subclass. *MAF* (16q23) is a basic zipper transcription factor that belongs to a subfamily of large MAF proteins and interacts with other transcription factors with the basic zipper motif to mediate both gene activation and repression. It is believed to act as an oncogene after undergoing translocation with the IgH locus (14q32) (Chesi et al., 1998). This translocation is observed in ∼ 2% of multiple myelomas. MAF is believed to interact with Cyclin D2 which is overexpressed in cases with translocations leading to increased tumor proliferation, and a poorer clinical outcome. Although the molecular mechanisms of MAF proteins are not well understood, one study reports that overexpression of *MAF* leads to down-regulation of *BCL2* expression and increase in apoptosis upon interaction with *MYB* (Peng et al., 2007). The fact that this gene is down-regulated in our

dataset suggests that cell viability is enhanced in tumors with *MAF* deletion. This is further supported by the fact that MAF has a tumor suppressor role because it participates in TP53-mediated cell death (Hale et al., 2000). *MAFA,* a member of the MAF family, maps to the frequently amplified 8q24.3 region found in prostate cancer (Saramaki and Visakorpi, 2007), hence suggesting a different mode of action for this member of the MAF subfamily. Interestingly, MAFB, another member of this subfamily, interacts with the ETS transcription factor ETS1 to inhibit erythroid differentiation (Sieweke et al., 1996). Hence, it appears that the deletion of the *MAF* tumor suppressor gene in the *ERG*-rearranged subclass facilitates tumor progression by inhibition of the apoptotic pathways.

The second *ERG*-rearranged cancer-specific aberration, amplification of 7q, is one of the earliest reported chromosomal events associated with prostate cancer (Saramaki and Visakorpi, 2007). In particular, recent studies have demonstrated amplification of *MCM7* in ∼ 50% of aggressive prostate cancers and 20% in indolent tumors (Ren et al., 2006). They also demonstrated a good correlation between transcript expression, protein expression, and gene amplification of *MCM7*. A recent study demonstrated *MCM7* as being significantly associated with prostate cancer progression (Laitinen et al., 2008). *MCM7* is part of a complex of genes that plays a key role in controlling DNA replication (Homesley et al., 2000) and has been implicated to be involved in tumorigenesis (Honeycutt et al., 2006). No previous evidence has been reported on association of *ERG*-rearranged prostate cancer with gain of 7q. We also found a corresponding up-regulation of the transcript expression in our samples. Interestingly, the *MCM7* gene also contains a microRNA *miR-106b-25* cluster which is overexpressed in prostate cancer (Ambs et al., 2008). *miR-106b-25* acts as a modulator of the *TGFβ* pathway where it suppresses the expression of *CDKN1A* (p21), a cell cycle inhibitor downstream of *TGFβ* which is also a target of *MYC*. Because *MYC* is seen to be amplified in prostate cancer, it suggests a co-operative effect at the genomic level that leads to inhibition of the *TGFβ* tumor suppressor pathway. In addition, the transcription factor *E2F1* regulates the expression of both *MCM7* and *miR-106b-25*. *E2F1* in turn is regulated by *miR-106b-25* in a negative feedback loop. Hence, it remains to be established if overexpression of the miRNA or amplification of *MCM7* or both contributes to the oncogenic event at this locus. If indeed the miRNA is involved in tumor progression, antisense oligos designed against *miR-106b-25* would be the potential candidates to treat tumors with *ERG* rearrangement.

The nonrearranged cancers showed enrichment for deletion in 6q. Studies have reported a deletion frequency of 24–50% (Alers et al., 2001; El Gedaily et al., 2001). *SNX14*, which maps to this region, was seen to have a single copy deletion by FISH. A corresponding reduction in transcript expression was seen in the nonrearranged cases. SNX14 is associated with the endoplasmic reticulum and may play a role in receptor trafficking (Carroll et al., 2001). The protein contains a regulator of G protein signaling (RGS) domain. This is the first report of association of this gene with prostate cancer. In addition, analysis of the *ERG* rearrangement associated gene expression signature showed an enrichment of upregulated genes mapping to 6q in the *ERG* rearranged subclass. Among the 6q genes that showed striking differences between rearranged and nonrearranged cancer was *MYO6*, which is preferentially expressed in rearranged cancers. MYO6 is an actin motor involved in intracellular vesicle trafficking and transport. It was proposed to be an early marker for prostate cancer because its expression was seen to be high in PIN lesions. It has been suggested that overexpression of *MYO6* may promote tumor growth and invasion (Knudsen, 2006). It has also been demonstrated to be associated with distinct changes in the Golgi apparatus and is coexpressed with *GOLM1* (Golgi membrane protein 1), a gene involved in prostate cancer progression (Wei et al., 2008). Hence, the genes at this locus appear to be involved in the modulation of protein trafficking.

In determining the frequency of molecular alterations using SNP array analysis, one important limitation has to do with the issue of sampling. The SNP array data used in the current study interrogates pools of tumor cells that also contain other cell types such as endothelial and stromal cells. The FISH assays are able to assess a specific genomic result—albeit at a lower resolution—on individual cells. We would view the FISH data presented in the current study as the Gold Standard and the SNP data as the hypothesis generating whole genome discovery dataset. Future studies using the FISH assays developed in this study for validation on larger clinical cohorts will be better suited to address the actual frequency of the lesions found to be associated with *ERG* rearrangement.

Our observation on associations between *ERG* rearranged prostate cancer and 16q and 6q

alterations is consistent with the results from Lapointe et al. (2007), where 16q deletion is in the same category as *TMPRSS2-ERG* fusion by deletion whereas 6q deletion is found in the less aggressive subtype. Previously, Tomlins et al. (2007) reported on the enrichment of ETS fusion prostate cancer-related genes on 6q21 using ETS overexpression as a surrogate for ETS rearrangements. They suggested a cooperative amplification at 6q21 in ETS rearranged tumors or loss of 6q21 in ETS nonrearranged tumors and hypothesized that down-regulation of genes at 6q21 may be important to tumor development in ETS nonrearranged prostate cancers. Here, we present direct evidence of association of 6q DNA copy number alteration with the prostate cancer subclasses and the corresponding deregulation of gene expression. Interestingly, the reported frequencies of all of the *ERG*-rearranged cancer specific genomic alterations identified by our study are in agreement with the frequencies of *TMPRSS2-ERG* fusion incidence.

We originally introduced the break apart assay for *ERG* rearrangements (Tomlins et al., 2005) because the genomic distance between *TMPRSS2* and *ERG* was 3 MB (Perner et al., 2006) and thus too small to develop a reliable fusion assay using BAC probe-based FISH. However, the *ERG* break-apart assay only indirectly assesses that *ERG* is fused to *TMPRSS2*. In the vast majority of cases, *ERG* break apart is a surrogate for *TMPRSS2-ERG* gene fusion as previously demonstrated by RT-PCR (Tomlins et al., 2005). One limitation of the *ERG* break apart assay is that other five prime partners than *TMPRSS2* could give the same result. Based on the unpublished observations, we estimate that this may occur in at most 5–10% of cases with *ERG* rearrangement. Specifically, we have seen *ERG* break apart with *SLC45A3* being the five prime partner in 5% of over 550 prostate cancer cases analyzed on a clinical cohort from Berlin. Therefore, while *ERG* break apart is an indirect assay, it only misclassifies a small percentage of cases. The parallel use of other break apart assays targeting the five prime partners such as *TMPRSS2* and *SLC45A3* would help to clarify these cases.

The use of custom tiling arrays further allowed us to interrogate the various ETS genes. Some of the ETS genes showed changes in the *TMPRSS2-ERG* fusion positive samples tested. One of the aberrations involved a complete/partial deletion of *ETV6*. The product of *ETV6* contains two functional domains: an N-terminal pointed (PNT) domain that is involved in the protein–protein interactions with itself and other proteins, and a COOH-terminal DNA-binding domain. Gene knockout studies in mice suggest that it is required for hematopoiesis and maintenance of the developing vascular network. This gene is known to be involved in a large number of chromosomal rearrangements associated with leukemia and congenital fibrosarcoma. This gene has been reported to be frequently deleted or mutated in prostate cancer (Kibel et al., 2002), suggesting that it may act as a tumor suppressor with inactivation leading to cancer progression. The tiling array also proved to be an efficient method for mapping the exact *TMPRSS2-ERG* fusion breakpoints. In the case of *EWS* rearrangements in leukemia, the genomic breakpoints have been determined to be tightly clustered for the *EWS* locus (<8 Kb region), whereas the breakpoints of its partner *FLI1*, occurs over a larger 35 Kb region in Ewing's family tumors (Delattre et al., 1992). To date, 12 distinct *EWS-FLI1* rearrangements have been described each containing variable combinations of exons flanking the DNA fusion point (Zucman et al., 1993; Zoubek et al., 1994). Therefore, even within a specific *EWS* rearrangement subclass such as *EWS-FLI1*, slightly different fusion proteins are produced. The result may lead to variations in the protein fusion product with respect to protein structure and activity as an oncogene. From a clinical perspective, these variant fusion proteins may be associated with different prognostic significance (Zoubek et al., 1996; de Alava et al., 1998).

Hence using high resolution arrays, we were able to determine the genomic alterations specific to the ETS fusion subclass of prostate cancer. The approach of combining the genomic data with the gene expression will facilitate a better understanding of the molecular mechanisms that lead to tumor progression.

ACKNOWLEDGMENTS

REFERENCES

Alers JC, Krijtenburg PJ, Vis AN, Hoedemaeker RF, Wildhagen MF, Hop WC, van Der Kwast TT, Schroder FH, Tanke HJ, van Dekken H. 2001. Molecular cytogenetic analysis of prostatic adenocarcinomas from screening studies: Early cancers

may contain aggressive genetic features. Am J Pathol 158:399–406.

Ambs S, Prueitt RL, Yi M, Hudson RS, Howe TM, Petrocca F, Wallace TA, Liu CG, Volinia S, Calin GA, Yfantis HG, Stephens RM, Croce CM. 2008. Genomic profiling of microRNA and messenger RNA reveals deregulated microRNA expression in prostate cancer. Cancer Res 68:6162–6170.

Amin MB, Grignon DJ, Humphrey PA, Srigley JR. 2003. Gleason Grading of Prostate Cancer: A Contemporary Approach, 1st ed. Philadelphia: Lippincott Williams and Wilkins, p. 116.

Attard G, Clark J, Ambroisine L, Fisher G, Kovacs G, Flohr P, Berney D, Foster CS, Fletcher A, Gerald WL, Moller H, Reuter V, De Bono JS, Scardino P, Cuzick J, Cooper CS. 2008. Duplication of the fusion of TMPRSS2 to ERG sequences identifies fatal human prostate cancer. Oncogene 27:253–263.

Beroukhim R, Getz G, Nghiemphu L, Barretina J, Hsueh T, Linhart D, Vivanco I, Lee JC, Huang JH, Alexander S, Du J, Kau T, Thomas RK, Shah K, Soto H, Perner S, Prensner J, Debiasi RM, Demichelis F, Hatton C, Rubin MA, Garraway LA, Nelson SF, Liau L, Mischel PS, Cloughesy TF, Meyerson M, Golub TA, Lander ES, Mellinghoff IK, Sellers WR. 2007. Assessing the significance of chromosomal aberrations in cancer: Methodology and application to glioma. Proc Natl Acad Sci USA 104:20007–20012.

Carroll P, Renoncourt Y, Gayet O, De Bovis B, Alonso S. 2001. Sorting nexin-14, a gene expressed in motoneurons trapped by an in vitro preselection method. Dev Dyn 221:431–442.

Chesi M, Bergsagel PL, Shonukan OO, Martelli ML, Brents LA, Chen T, Schrock E, Ried T, Kuehl WM. 1998. Frequent dysregulation of the c-maf proto-oncogene at 16q23 by translocation to an Ig locus in multiple myeloma. Blood 91:4457–4463.

de Alava E, Kawai A, Healey JH, Fligman I, Meyers PA, Huvos AG, Gerald WL, Jhanwar SC, Argani P, Antonescu CR, Pardo-Mindan FJ, Ginsberg J, Womer R, Lawlor ER, Wunder J, Andrulis I, Sorensen PH, Barr FG, Ladanyi M. 1998. EWS-FLI1 fusion transcript structure is an independent determinant of prognosis in Ewing's sarcoma. J Clin Oncol 16:1248–1255.

Delattre O, Zucman J, Plougastel B, Desmaze C, Melot T, Peter M, Kovar H, Joubert I, de Jong P, Rouleau G, Aurias A, Thomas G. 1992. Gene fusion with an ETS DNA-binding domain caused by chromosome translocation in human tumours. Nature 359:162–165.

Demichelis F, Fall K, Perner S, Andren O, Schmidt F, Setlur SR, Hoshida Y, Mosquera JM, Pawitan Y, Lee C, Adami HO, Mucci LA, Kantoff PW, Andersson SO, Chinnaiyan AM, Johansson JE, Rubin MA. 2007. TMPRSS2:ERG gene fusion associated with lethal prostate cancer in a watchful waiting cohort. Oncogene 26:4596–4599.

Demichelis F, Greulich H, Macoska JA, Beroukhim R, Sellers WR, Garraway L, Rubin MA. 2008. SNP panel identification assay (SPIA): A genetic-based assay for the identification of cell lines. Nucleic Acids Res 36:2446–2456.

El Gedaily A, Bubendorf L, Willi N, Fu W, Richter J, Moch H, Mihatsch MJ, Sauter G, Gasser TC. 2001. Discovery of new DNA amplification loci in prostate cancer by comparative genomic hybridization. Prostate 46:184–190.

Greenlee RT, Hill-Harmon MB, Murray T, Thun M. 2001. Cancer statistics, 2001. CA Cancer J Clin 51:15–36.

Hale TK, Myers C, Maitra R, Kolzau T, Nishizawa M, Braithwaite AW. 2000. Maf transcriptionally activates the mouse p53 promoter and causes a p53-dependent cell death. J Biol Chem 275:17991–17999.

Helgeson BE, Tomlins SA, Shah N, Laxman B, Cao Q, Prensner JR, Cao X, Singla N, Montie JE, Varambally S, Mehra R, Chinnaiyan AM. 2008. Characterization of TMPRSS2:ETV5 and SLC45A3:ETV5 gene fusions in prostate cancer. Cancer Res 68:73–80.

Hofer MD, Kuefer R, Huang W, Li H, Bismar TA, Perner S, Hautmann RE, Sanda MG, Gschwend JE, Rubin MA. 2006. Prognostic factors in lymph node-positive prostate cancer. Urology 67:1016–1021.

Homesley L, Lei M, Kawasaki Y, Sawyer S, Christensen T, Tye BK. 2000. Mcm10 and the MCM2-7 complex interact to initiate DNA synthesis and to release replication factors from origins. Genes Dev 14:913–926.

Honeycutt KA, Chen Z, Koster MI, Miers M, Nuchtern J, Hicks J, Roop DR, Shohet JM. 2006. Deregulated minichromosomal maintenance protein MCM7 contributes to oncogene driven tumorigenesis. Oncogene 25:4027–4032.

Hupe P, Stransky N, Thiery JP, Radvanyi F, Barillot E. 2004. Analysis of array CGH data: From signal ratio to gain and loss of DNA regions. Bioinformatics 20:3413–3422.

Kibel AS, Faith DA, Bova GS, Isaacs WB. 2002. Mutational analysis of ETV6 in prostate carcinoma. Prostate 52:305–310.

Knudsen B. 2006. Migrating with myosin VI. Am J Pathol 169:1523–1526.

Korbel JO, Urban AE, Grubert F, Du J, Royce TE, Starr P, Zhong G, Emanuel BS, Weissman SM, Snyder M, Gerstein MB. 2007. Systematic prediction and validation of breakpoints associated with copy-number variants in the human genome. Proc Natl Acad Sci USA 104:10110–10115.

Laitinen S, Martikainen PM, Tolonen T, Isola J, Tammela TL, Visakorpi T. 2008. EZH2, Ki-67 and MCM7 are prognostic markers in prostatectomy treated patients. Int J Cancer 122:595–602.

Lapointe J, Li C, Giacomini CP, Salari K, Huang S, Wang P, Ferrari M, Hernandez-Boussard T, Brooks JD, Pollack JR. 2007. Genomic profiling reveals alternative genetic pathways of prostate tumorigenesis. Cancer Res 67:8504–8510.

Leprince D, Gegonne A, Coll J, de Taisne C, Schneeberger A, Lagrou C, Stehelin D. 1983. A putative second cell-derived oncogene of the avian leukaemia retrovirus E26. Nature 306:395–397.

Li C, Hung Wong W. 2001. Model-based analysis of oligonucleotide arrays: Model validation, design issues and standard error application. Genome Biol 2:RESEARCH0032.

Liu W, Chang B, Sauvageot J, Dimitrov L, Gielzak M, Li T, Yan G, Sun J, Adams TS, Turner AR, Kim JW, Meyers DA, Zheng SL, Isaacs WB, Xu J. 2006. Comprehensive assessment of DNA copy number alterations in human prostate cancers using Affymetrix 100K SNP mapping array. Genes Chromosomes Cancer 45:1018–1032.

Matsuyama H, Pan Y, Yoshihiro S, Kudren D, Naito K, Bergerheim US, Ekman P. 2003. Clinical significance of chromosome 8p, 10q, and 16q deletions in prostate cancer. Prostate 54:103–111.

Mertz KD, Setlur SR, Dhanasekaran SM, Demichelis F, Perner S, Tomlins S, Tchinda J, Laxman B, Vessella RL, Beroukhim R, Lee C, Chinnaiyan AM, Rubin MA. 2007. Molecular characterization of TMPRSS2-ERG gene fusion in the NCI-H660 prostate cancer cell line: A new perspective for an old model. Neoplasia 9:200–206.

Mosquera JM, Perner S, Demichelis F, Kim R, Hofer MD, Mertz KD, Paris PL, Simko J, Collins C, Bismar TA, Chinnaiyan AM, Rubin MA. 2007. Morphological features of TMPRSS2-ERG gene fusion prostate cancer. J Pathol 212:91–101.

Peng S, Lalani S, Leavenworth JW, Ho IC, Pauza ME. 2007. c-Maf interacts with c-Myb to down-regulate Bcl-2 expression and increase apoptosis in peripheral CD4 cells. Eur J Immunol 37:2868–2880.

Perner S, Demichelis F, Beroukhim R, Schmidt FH, Mosquera JM, Setlur S, Tchinda J, Tomlins SA, Hofer MD, Pienta KG, Kuefer R, Vessella R, Sun XW, Meyerson M, Lee C, Sellers WR, Chinnaiyan AM, Rubin MA. 2006. TMPRSS2:ERG fusion-associated deletions provide insight into the heterogeneity of prostate cancer. Cancer Res 66:8337–8341.

Ren B, Yu G, Tseng GC, Cieply K, Gavel T, Nelson J, Michalopoulos G, Yu YP, Luo JH. 2006. MCM7 amplification and overexpression are associated with prostate cancer progression. Oncogene 25:1090–1098.

Royce TE, Rozowsky JS, Gerstein MB. 2007. Assessing the need for sequence-based normalization in tiling microarray experiments. Bioinformatics 23:988–997.

Saramaki O, Visakorpi T. 2007. Chromosomal aberrations in prostate cancer. Front Biosci 12:3287–3301.

Saramaki OR, Porkka KP, Vessella RL, Visakorpi T. 2006. Genetic aberrations in prostate cancer by microarray analysis. Int J Cancer 119:1322–1329.

Setlur SR, Mertz KD, Hoshida Y, Demichelis F, Lupien M, Perner S, Sboner A, Pawitan Y, Andren O, Johnson LA, Tang J, Adami HO, Calza S, Chinnaiyan AM, Rhodes D, Tomlins S, Fall K, Mucci LA, Kantoff PW, Stampfer MJ, Andersson SO, Varenhorst E, Johansson JE, Brown M, Golub TR, Rubin MA. 2008. Estrogen-dependent signaling in a molecularly distinct subclass of aggressive prostate cancer. J Natl Cancer Inst 100:815–825.

Sieweke MH, Tekotte H, Frampton J, Graf T. 1996. MafB is an interaction partner and repressor of Ets-1 that inhibits erythroid differentiation. Cell 85:49–60.

Tomlins SA, Rhodes DR, Perner S, Dhanasekaran SM, Mehra R, Sun XW, Varambally S, Cao X, Tchinda J, Kuefer R, Lee C,

Montie JE, Shah RB, Pienta KJ, Rubin MA, Chinnaiyan AM. 2005. Recurrent fusion of TMPRSS2 and ETS transcription factor genes in prostate cancer. Science 310:644–648.

Tomlins SA, Mehra R, Rhodes DR, Smith LR, Roulston D, Helgeson BE, Cao X, Wei JT, Rubin MA, Shah RB, Chinnaiyan AM. 2006. TMPRSS2:ETV4 gene fusions define a third molecular subtype of prostate cancer. Cancer Res 66:3396–3400.

Tomlins SA, Laxman B, Dhanasekaran SM, Helgeson BE, Cao X, Morris DS, Menon A, Jing X, Cao Q, Han B, Yu J, Wang L, Montie JE, Rubin MA, Pienta KJ, Roulston D, Shah RB, Varambally S, Mehra R, Chinnaiyan AM. 2007. Distinct classes of chromosomal rearrangements create oncogenic ETS gene fusions in prostate cancer. Nature 448:595–599.

Urban AE, Korbel JO, Selzer R, Richmond T, Hacker A, Popescu GV, Cubells JF, Green R, Emanuel BS, Gerstein MB, Weissman SM, Snyder M. 2006. High-resolution mapping of DNA copy alterations in human chromosome 22 using high-density tiling oligonucleotide arrays. Proc Natl Acad Sci USA 103:4534–4539.

Watson JE, Doggett NA, Albertson DG, Andaya A, Chinnaiyan A, van Dekken H, Ginzinger D, Ha C, James K, Kamkar S, Kowbel D, Pinkel D, Schmitt L, Simko JP, Volik S, Weinberg VK, Paris PL, Collins C. 2004. Integration of high-resolution array comparative genomic hybridization analysis of chromosome 16q with expression array data refines common regions of loss at 16q23-qter and identifies underlying candidate tumor suppressor genes in prostate cancer. Oncogene 23:3487–3494.

Wei S, Dunn TA, Isaacs WB, De Marzo AM, Luo J. 2008. GOLPH2 and MYO6: Putative prostate cancer markers localized to the Golgi apparatus. Prostate 68:1387–1395.

Yoshimoto M, Cunha IW, Coudry RA, Fonseca FP, Torres CH, Soares FA, Squire JA. 2007. FISH analysis of 107 prostate cancers shows that PTEN genomic deletion is associated with poor clinical outcome. Br J Cancer 97:678–685.

Zoubek A, Pfleiderer C, Salzer-Kuntschik M, Amann G, Windhager R, Fink FM, Koscielniak E, Delattre O, Strehl S, Ambros PF. 1994. Variability of EWS chimaeric transcripts in Ewing tumours: A comparison of clinical and molecular data. Br J Cancer 70:908–913.

Zoubek A, Dockhorn-Dworniczak B, Delattre O, Christiansen H, Niggli F, Gatterer-Menz I, Smith TL, Jurgens H, Gadner H, Kovar H. 1996. Does expression of different EWS chimeric transcripts define clinically distinct risk groups of Ewing tumor patients? J Clin Oncol 14:1245–1251.

Zucman J, Melot T, Desmaze C, Ghysdael J, Plougastel B, Peter M, Zucker JM, Triche TJ, Sheer D, Turc-Carel C, Ambros P, Combaret V, Lenoir G, Aurias A, Thomas G, Delattre O. 1993. Combinatorial generation of variable fusion proteins in the Ewing family of tumours. EMBO J 12:4481–4487.